Specificity of *Campylobacter jejuni* Adhesin PEB3 for Phosphates and Structural Differences among Its Ligand Complexes[†,‡]

Tongpil Min,[§] Masoud Vedadi,[||] David C. Watson,[⊥] Gregory A. Wasney,[||] Christine Munger,[§] Miroslaw Cygler,[§,@] Allan Matte,*[,@] and N. Martin Young*[,⊥]

Department of Biochemistry, McGill University, Montreal, QC, H3G 1Y6 Canada, Structural Genomics Consortium, University of Toronto, and Institute for Biological Sciences, National Research Council of Canada, Ottawa, ON, K1A 0R6 Canada, and Biotechnology Research Institute, National Research Council of Canada, Montreal, QC, H4P 2R2 Canada

Received November 28, 2008; Revised Manuscript Received February 13, 2009

ABSTRACT: PEB3 is a glycoprotein adhesin from *Campylobacter jejuni* whose structure suggested a role in transport. We have investigated potential ligands for PEB3 and characterized their binding properties using biophysical methods in solution and by X-ray crystallography. A thermal aggregation assay of PEB3 with a library of physiological compounds identified three possible ligands [3-phosphoglycerate (3-PG), phosphoenolpyruvate (PEP), and aconitate], which stabilized wild-type PEB3 but did not stabilize either a PEB3 form containing two mutations at the ligand-binding site, T138A/S139A, or a second PEB3 mutant, K135E, at a site ~14 Å away. Fluorescence titration experiments and cocrystal structures with various ligands were used to characterize the binding of 3-PG, PEP, and phosphate to PEB3. Further, a *C. jejuni* growth experiment in minimal medium supplemented with 3-PG showed that this molecule enhances the growth of wild-type *C. jejuni*, but not of the PEB3 mutants. Crystallographic analysis of PEB3 complexes revealed that the Ser171−Gln180 region in the presence of 3-PG or other phosphates is helical and similar to those of other transport proteins, but it is nonhelical when citrate is bound. The K135E mutation resulted in expression of a more highly glycosylated form of PEB3 in vivo, and its crystal structure showed the conformation of the first two residues of the glycan. On the basis of our findings, we suggest that PEB3 is a transport protein that may function in utilization of 3-PG or other phosphate-containing molecules from the host.

Campylobacter jejuni adhesin PEB3 (Cj0289c) is one of more than 30 proteins that have been shown to be N-glycosylated in vivo by the *pgl* system (*1, 2*). The oligosaccharyltransferase PglB of this system attaches a heptasaccharide to Asn90 of PEB3, which is within the consensus sequon sequence, D/E-X-N-X-S/T (*2*). Crystallographic studies of PEB3 (*3*) showed that its sequon is located within a surface-exposed loop, suggesting that PglB could modify Asn90 when PEB3 is in its folded state. The structure also showed that PEB3 contains a centrally located ligand-binding cleft that was occupied by a citrate molecule from the crystallization medium. Citrate is unlikely to be PEB3′s natural ligand since another gene, *cj0203*, has been identified to encode a citrate transporter in the genome of *C. jejuni* (*4*). The overall structure of PEB3 is that of a dimer and is similar to those of other type II periplasmic transport proteins (*3*). The closest structural homologues of PEB3 are transporters for molybdate/tungstate, sulfate, and ferric iron, suggesting the natural ligand would be a di- or trianion or cation. Alternatively, the ligand-binding site might recognize a cell surface molecule on a host cell to provide adhesion. In the case of *C. jejuni* PEB1a, the protein has both adhesin and transport capabilities (*5*), so a similar dual function is also possible for PEB3. However, no experimental data have so far been reported in support of PEB3 functioning as a transporter, or of possible ligands that could originate from host cells.

To identify potential ligands for PEB3 in its role as either an adhesin or a transporter, we applied two recently developed techniques that permitted the interrogation of relevant compound libraries. These were a glycan microarray for the adhesin role (*6*) and a protein stabilization (T_{agg}) assay with a library of physiologically relevant ligands (*7, 8*). The latter study reveals that PEB3 recognizes 3-phosphoglycerate and other molecules found in intermediary metabolism of cells, including those of eukaryotic hosts. Fluorescence spectroscopy was used to characterize the binding properties

[†] This work was supported in part by CIHR Grant GSP-48370 (M.C. and A.M.). Use of the Advanced Photon Source was supported by the U.S. Department of Energy, Office of Science, Office of Basic Energy Sciences, under Contract DE-AC02-06CH11357. Use of the SGX Collaborative Access Team (SGX-CAT) beamline facilities at Sector 31 of the Advanced Photon Source was provided by SGX Pharmaceuticals, Inc., who constructed and operates the facility.

[‡] Coordinates for the structures described in this paper have been deposited in the Protein Data Bank as entries 3FJG, 3FJ7, 3FJM, and 3FIR.

* To whom correspondence should be addressed. N.M.Y.: phone, (613) 990-0855; fax, (613) 941-1327; e-mail, martin.young@nrc-cnrc.gc.ca. A.M.: phone, (514) 496-2557; fax, (514) 496-5143; e-mail, allan.matte@bri.nrc.ca.

[§] McGill University.

[||] University of Toronto.

[⊥] Institute for Biological Sciences, National Research Council of Canada.

[@] Biotechnology Research Institute, National Research Council of Canada.

10.1021/bi802195d CCC: $40.75
Published on Web 02/23/2009

of phospho ligands to PEB3, and the structures of its complexes with 3-phosphoglycerate and other ligands were determined by X-ray crystallography. These structures showed a significant conformational difference in the Ser171−Gln180 region of the binding site compared to the previously determined citrate complex. We further show that the 3-phosphoglycerate ligand enhanced the growth of *C. jejuni* in a minimal medium, while cells with PEB3 binding site mutants were unaffected. Our findings therefore suggest that one biological role for PEB3 may be to facilitate the growth of *C. jejuni* within host cells by transporting phosphorylated compounds from the cytoplasm into the bacterium. We also determined the structure of an inactive mutant of PEB3, K135E, which was more completely glycosylated than the wild type when reintroduced into *C. jejuni*, and the disaccharide portion of the glycan could be seen in the crystal structure.

EXPERIMENTAL PROCEDURES

Site-Directed Mutagenesis of PEB3. The *cj0289c* gene of *C. jejuni* 11168 cloned with a C-terminal His_6 tag (*3*) was mutagenized using a two-stage mutagenesis protocol. Forward and reverse PCR primers both containing the desired mutation were used in separate PCRs in conjunction with the 5′ and 3′ gene primers to generate two overlapping gene fragments. Both PCR products were then used as a template in a third PCR with the primer pair designed to generate a full-length *peb3* product without the periplasmic leader sequence and a six-His tag at the 3′ end of the gene. Full-length mutagenized PCR products were subsequently cloned and verified by sequence analysis. A single mutation, K135E, and a double mutant, T138A/S139A, were constructed using the following primer pairs: Peb3 T138A/S139A, GGAAAGAGCAATGCTGCTGGAACTGGAG (forward) and CTCCAGTTCCAGCAGCATTGCTCTTTCC (reverse); PEB3 K135E, CCTGAAGGTGCTGGAGAGAGCAATACTTCTGG (forward) and CCAGAAGTATTGCTCTCTCCAGCACCTTCAGG (reverse).

Expression of Proteins in Escherichia coli. Wild-type and mutant proteins were overexpressed in *E. coli* AD202 cells from a 1 L culture and lysed by mechanical disruption in 10 mM HEPES buffer (pH 7.5). Protein extracts were clarified by centrifugation (27000*g* for 30 min at 4 °C), and cell debris was discarded. Total membrane and soluble protein fractions were obtained from clarified cell extracts by centrifugation (100000*g* for 60 min at 4 °C). Following adjustment of the lysate to 500 mM NaCl and 50 mM imidazole, wild-type and mutant proteins were purified from the soluble fractions by IMAC as previously described (*3*).

Genetic Manipulations of PEB3 in C. jejuni. Construction of allelic replacements was performed in three stages. The kanamycin resistance gene from pUC4K (GE Healthcare) was liberated from the plasmid as a *Sal*I fragment. The *peb3* structural gene and its 3′ downstream region were amplified from *C. jejuni* NCTC 11168 by PCR using Expand polymerase as described by the manufacturer (Roche Diagnostics). The *C. jejuni peb3* allele was mutagenized using a two-stage PCR mutagenesis protocol as described above. PCR products were used as template with the primers 5′-GCTAGCTAGGCATGCATGAAAAAAATTATTACTTTATTTGGTGCATG-3′ (forward), 5′-GCTAGCTAGGTCGACTTAGTGATGGTGATGGTGATGTTCTCTCCAGCCGTATTTTTTAAAAATTTC-3′ (His6x reverse) to generate full-length, mutated *peb3* K135E with a His_6 tag, for protein purification purposes, at the 3′ end of the gene, and 5′-GCTAGCTAGGTCGACTTCTCTCCAGCCGTATTTTTTAAAAATTTC-3′ to generate *peb3* T138A/S139A with no His tag, since the construct bearing this double mutation was intended for use in allelic exchange only and not for subsequent glycoprotein purification purposes. The primers for the *peb3* downstream flanking sequence (3′ end) of the coding sequence were 5′-GCTAGCTAGGTCGACACCTTCATACACGCTTTTTAGCGTGTATTC-3′ and 5′-GCTAGCTAGGAATTCCCATAAACTTCTAATTTTTCAAGATTAAATG-3′. The plasmid construct for the gene replacement was assembled in the following steps. The pUC18 vector was digested with *Sph*I and *Sal*I and purified for use as a cloning vector. A single fragment ligation was performed with the mutagenized *peb3* (*Sph*I- and *Sal*I-digested) and the pUC18 vector (*Sph*I/*Sal*I). Once this construct was verified by sequence analysis of the mutagenized *peb3* insert, the 3′ flanking sequence (*Sal*I/*Eco*RI-digested) was inserted into the *Sal*I/*Eco*RI-digested plasmid construct containing mutagenized *peb3* in a second single-fragment ligation. Following verification of the resulting construct, the kanamycin resistance marker was inserted between the structural gene and the 3′ flanking sequence. The recombinant plasmids were propagated in *E. coli* DH12S and introduced into *C. jejuni* NCTC 11168 by electroporation. Mutant clones were screened for kanamycin resistance and subsequently verified by PCR from genomic DNA followed by sequence analysis.

Preparation of Wild-Type and Mutant PEB3 Glycoproteins. Wild-type and K135E mutant *C. jejuni* cells bearing His_6 purification tags from two plates of overnight growth were resuspended in 10 mL of Mueller Hinton (MH) broth and used to inoculate 1.5 L of MH medium. Cultures were grown under microaerophilic conditions at 37 °C for 24 h with shaking at 120 rpm. Bacterial cells from 6 L of culture medium were harvested by centrifugation (10000*g* for 15 min at 4 °C) and immediately frozen at −75 °C. Frozen cell pellets were thawed on ice in 0.2 M glycine-HCl buffer (pH 2.2) and proteins extracted for 30 min with gentle stirring. Protein extracts were clarified by centrifugation (27000*g* for 30 min at 4 °C), adjusted to pH 7.5, and dialyzed against 500 mM NaCl, 10 mM HEPES buffer (pH 7.5), and 50 mM imidazole. Mutagenized PEB3 protein was subsequently purified by IMAC as described above and analyzed by SDS−PAGE followed by immunoblotting with an SBA−alkaline phosphatase reagent to identify glycosylated proteins, as previously described (*1*).

Identification of Ligands by Differential Static Light Scattering (DSLS)[1]. Ligand binding was detected by monitoring the increase in the thermostability of proteins in the presence of ligands, using StarGazer technology (Harbinger Biotech) to monitor protein aggregation by DSLS (*8*). Protein samples (50 μL) at 0.4 mg/mL were heated from 27 to 80 °C at a rate of 0.5 °C/min in clear-bottom 384-well plates (Nunc, Thermo Fisher Scientific) in 50 μL of 100 mM Hepes

[1] Abbreviations: Bac, 2,4-diamino-2,4,6-trideoxy-D-Glc; DSLS, differential static light scattering; PDB, Protein Data Bank; L-PL, L-phospholactate; 3-PG, 3-phosphoglycerate; PEP, phosphoenolpyruvate.

(pH 7.5) and 150 mM NaCl, with a final concentration of the test compound of 1 mM. Protein aggregation was monitored by capturing images of scattered light every 30 s with a charge-coupled device camera. The pixel intensities in a preselected region of each well were integrated to generate a value representative of the total amount of scattered light in that region. These total intensities were then plotted against temperature for each sample well and fit to the Boltzman equation by nonlinear regression. The point of inflection of each "denaturation" curve was identified as T_{agg} (aggregation temperature). The increase in stability of the protein in the presence of a ligand is shown as ΔT_{agg}. The physiological compound library containing 163 compounds was prepared as previously described (*8*).

Ligand Titrations by Intrinsic Fluorescence. In the crystal structures of PEB3 without any added ligand, the ligand-binding site was found to be occupied by phosphate following overnight dialysis against 20 mM HEPES (pH 7.4) and 150 mM NaCl. However, phosphate was evidently replaced by citrate under the crystallization conditions that included 0.2 M diammonium hydrogen citrate, which showed a citrate molecule bound to PEB3 (*3*). To ensure that phosphate was removed from the ligand-binding site, 5 mL of PEB3 (3 mg/mL) was dialyzed twice against 2 L of 20 mM HEPES (pH 7.4), 150 mM NaCl, and 0.1 M diammonium hydrogen citrate. Next, to remove the citrate, the PEB3 sample was subjected to another cycle of extensive dialysis against 20 mM HEPES (pH 7.4) and 150 mM NaCl, and this preparation was used for the fluorescence experiments. Ligand binding assays by intrinsic protein fluorescence emission were performed using excitation at 290 nm and monitoring emission at 338 nm using a Spex Fluorolog 1681 spectrometer (Horiba Jobin Yvon Inc., Edison, NJ). The final volume change following addition of ligand was 3.1%. Ligand stock solutions were prepared at 5, 50, and 500 mM in Zeno-pure water and titrated into a 17 μM protein solution to a final ligand concentration of 2 mM. To confirm that the observed fluorescence signal changes were specific for PEB3, a 7.5 μM BSA solution was used as a control with a final concentration of each ligand of 2 mM. Data were fit to the equation $Y = X(T_{max} - T_0)/(K_d + X) + T_0$, where Y is the fluorescence intensity, X is the ligand concentration, T_{max} is the maximum fluorescence, T_0 is the minimum fluorescence, and K_d is the dissociation constant. Fitting was performed with MicroCal OriginPro version 7.0.

Effect of Ligands on Bacterial Growth. Growth experiments were performed as described for the Asp/Glu transporter, PEB1a (*5*). Liquid cultures of wild-type PEB3 and the two mutants were grown microaerobically at 120 rpm in either MH medium or the defined minimal medium MEM-α containing deoxyribonucleotides but no phenol red (Invitrogen). Overnight starter cultures grown in MH medium were used to inoculate triplicate, 1 mL samples of MEM-α containing 0, 1, or 5 mM 3-PG and 0.1 mM $FeSO_4$. After growth at 37 °C for 20 h, the absorbance of the cultures was measured at 600 nm with a model 40 Fisher Scientific cell density monitor (Fisher Scientific).

Cocrystallization and Structure Determination. Crystals of PEB3 with or without ligands were grown by hanging-drop vapor diffusion at 20 °C. Each drop contained 2 μL of protein (8−14 mg/mL) in buffer [20 mM HEPES (pH 7.4) and 150 mM NaCl] mixed with 2 μL of reservoir solution [18% (w/v) polyethylene glycol 3350 and 0.2 M diammonium hydrogen citrate], a slight modification of the original conditions (*3*). To obtain PEB3 crystals in the absence of bound citrate, the 0.2 M diammonium hydrogen citrate was replaced with 0.2 M ammonium acetate in the reservoir. For cocrystallization of PEB3 with various ligands, the 0.2 M diammonium hydrogen citrate was replaced with 0.2 M sodium phosphate, 0.2 M aconitate, 0.2 M PEP, or 0.2 M 3-PG in the drop, while keeping 0.2 M diammonium hydrogen citrate in the reservoir solution. All ligand solutions were adjusted to pH 5−5.5 prior to crystallization. This cocrystallization strategy was only successful in producing cocrystal structures of PEB3 with phosphate and 3-PG. To obtain additional complexes, PEB3 crystals grown in the presence of ammonium acetate were soaked in 2 mM aconitate or 2 mM PEP. Crystals of the glycosylated K135E mutant were grown in the original 0.2 M diammonium hydrogen citrate conditions (*3*). Due to the limited quantity of glycosylated, mutant protein available, cocrystallization or soaking with other ligands was not attempted.

Crystals were cryo-protected in reservoir solution supplemented with 15−20% (v/v) glycerol, picked up with a nylon loop, and flash-cooled by direct immersion of the crystals into liquid nitrogen. X-ray diffraction data were collected using either a Rigaku 007 Microfocus generator equipped with a HTC imaging plate detector (Molecular Structure Corp.) or at the 31-ID (SGX-CAT) beamline at the Advanced Photon Source (Argonne National Laboratory, Argonne, IL). Data sets were processed either using d*TREK (*9*) and Scala of the *CCP*4 suite (*10*) or using HKL2000 (*11*). The structures were determined by molecular replacement using AMoRe (*12*), using the coordinates of *C. jejuni* PEB3 (PDB entry 2HXW) as the search model. The structures were refined using REFAC5 (*13*) alternating with model building using COOT (*14*). Data collection and final refinement statistics are presented in Table 1, along with the RCSB Protein Data Bank (*15*) accession codes.

Thermal Stability of Glycosylated PEB3. A fluorescence microplate reader [FluoDia T70, Photon Technology International (Canada), London, ON] was used to measure the thermal stability of glycosylated K135E PEB3, and non-glycosylated K135E and wild-type PEB3, using binding of the fluorescent dye SYPRO Orange (Invitrogen) (*7, 8, 16, 17*). Both proteins were prepared in 20 mM HEPES (pH 7.4) and 150 mM NaCl and used at a final concentration of 2 μM in the presence of 1× SYPRO Orange. Fluorescence excitation was performed at 465 nm and the fluorescence emission recorded at 590 nm at 1 °C temperature increments from 23 to 75 °C. The resulting data were analyzed using the Levenberg−Marquardt nonlinear regression algorithm (Octave, http://www.octave.org). The inflection point (apparent T_m) was determined by fitting the data to the equation $f(T) = A + (B - A)/[1 + \exp(T_m - T)/C]$, where A is the fluorescence minimum, B is the fluorescence maximum, C is the rate of fluorescence change around the inflection point, and T is the temperature.

RESULTS

PEB3 Mutants. Two mutant forms of the protein were prepared for expression in *E. coli* and *C. jejuni*. One mutant had changes in two binding-site residues, T138A/S139A,

Table 1: X-ray Data Collection and Refinement Statistics

	3-PG	L-PL	phosphate	K135E
Data Collection Statistics				
space group	$P2_1$	$P2_12_12_1$	$P2_12_12_1$	$P2_1$
collection facility	HTC	ID31	ID31	ID31
cell dimensions				
a (Å)	61.92	62.23	62.42	49.58
b (Å)	85.70	79.24	79.65	101.96
c (Å)	100.17	99.05	98.39	56.81
α (deg)	90.00	90.00	90.00	90.00
β (deg)	90.04	90.00	90.00	108.9
γ (deg)	90.00	90.00	90.00	90.00
Z	4	8	8	4
resolution (Å)	44.9−2.2	43.9−1.7	18.7−1.6	20−2.0
wavelength (Å)	1.54	0.98	0.98	0.98
no. of observed reflections	310901	394978	430841	121375
no. of unique reflections	51009	54648	65094	35349
average redundancy	6.1	7.2	6.6	3.4
completeness (%)	96	100	99.2	98
R_{sym}[a]	0.065	0.083	0.067	0.085
$I/\sigma(I)$	19.5	11.6	15.8	17.1
Wilson *B*-factor	30.0	17.0	15.0	26.1
Refinement Statistics				
resolution (Å)	44.9−2.2	43.9−1.7	18.7−1.6	20−2.0
R_{work} (%)[b]	19.6	21.9	21.7	21.6
R_{free} (%)[c]	22.6	24.2	23.1	23.5
B-factor (Å^2)				
protein	24.4	12.9	12.5	35.0
ligand	22.8	12.6	8.6	39.6
solvent	28.1	21.8	22.4	45.4
glycan				51.2
Ramachandran plot				
allowed	100	100	100	99.8
generously allowed	0	0	0	0.2
disallowed	0	0	0	0
root-mean-square deviation				
bonds (Å)	0.004	0.003	0.003	0.006
angles (deg)	0.90	0.82	0.80	1.10
PDB entry	3FJG	3FJ7	3FJM	3FIR

[a] $R_{sym} = \sum|I_{obs} - I_{avg}|/\sum I_{avg}$. [b] $R_{work} = \sum|F_{obs} - F_{calc}|/\sum F_{obs}$. [c] $R_{free} = R_{work}$, except for a random test set of 5% of reflections not included in the refinement.

found to be critical for citrate recognition (*3*). The other mutant, K135E, was originally made prior to the structural work in an attempt to create a second glycosylation sequon at Asn137. Lys135 was subsequently shown to be ~14 Å from the citrate-binding site (*3*) and not in contact with the ligand. For in vitro experiments with ligands, the two mutants were expressed with C-terminal His_6 tags in *E. coli*. For in vivo experiments, the wild-type *peb3* gene in *C. jejuni* was replaced with the His_6-tagged form of K135E PEB3 or a T138A/S139A version without a His_6 tag.

Ligand Screening Using a Glycan Array. To identify possible cell surface glycans that might be recognized by PEB3 in its adhesin capacity, screening of Alexa Fluor-labeled PEB3 with a glycan array was carried out at the Core H facility of the Consortium for Functional Glycomics. Only one glycan exhibited reproducible binding with PEB3, a mannose 6-phosphate compound [deposited on the CFG site (*6*)]. This result was the first indication that PEB3 might have specificity for ligands containing phosphate moieties. Blotting experiments were therefore performed with representatives of the two types of eukaryotic glycoproteins that contain Man-6-P, i.e., lysosomal proteins and GPI-anchored proteins. However, both of these glycoproteins showed no reactivity with PEB3 (data not shown). Though it has been reported that PEB3 can bind to sulfated glycosaminoglycans (*18*), PEB3 showed no reactions with any of the sulfated oligosaccharides on the array, and sulfated component sugars of glycosaminoglycans also failed to stabilize the protein (see Screening for PEB3 Ligands by DSLS). Since PEB3 is a basic protein with a calculated pI of 9.3, the interaction with glycosaminoglycans may be charge-dependent and nonspecific.

Screening for PEB3 Ligands by DSLS. Screening wild-type PEB3 against a library of physiological ligands resulted in identification of two ligands that significantly stabilized PEB3 at a concentration of 1 mM, namely, 3-phosphoglycerate (3-PG) and aconitate. The effect of these ligands on T_{agg} was evaluated in more detail by titrating PEB3 with them (Figure 1A). Individual binding assays were also conducted with citrate, Man-6-P, diphosphoglycerate, phosphoenolpyruvate (PEP), and GalNAc 4- and 6-sulfates. Confirmatory experiments were also carried out with the PEB3 mutants K135E and T138A/S139A. The results showed that (a) citrate and Man-6-P were not behaving as ligands in this assay, (b) PEP acted as a ligand, and (c) the three active compounds, 3-PG, aconitate, and PEP, did not stabilize either of the two mutant proteins up to 5 mM. These mutant proteins themselves exhibited only small differences in T_{agg} compared to the wild type (62 °C), with values of 58 °C for K135E and 60 °C for the T138A/S139A protein. Therefore, the lack of thermal stabilization was not due to major changes in the intrinsic properties of the mutant proteins.

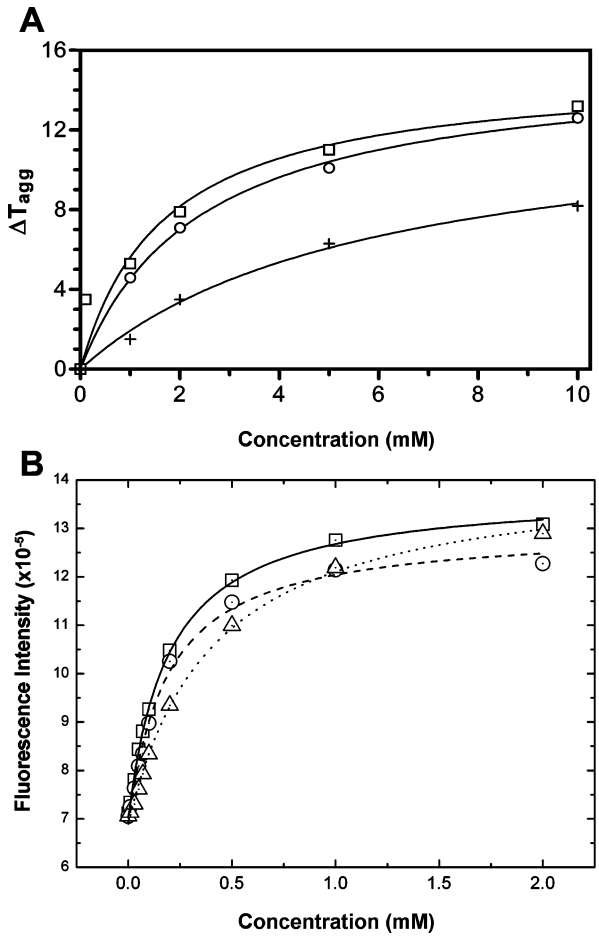

FIGURE 1: Thermal aggregation and fluorescence assays of PEB3 ligand binding. (A) Titration of 3-PG (□), PEP (○), and aconitate (+) against PEB3 evaluated by DSLS. (B) Effect of 3-PG (□), PEP (○), and phosphate (△) on the intrinsic fluorescence emission of PEB3.

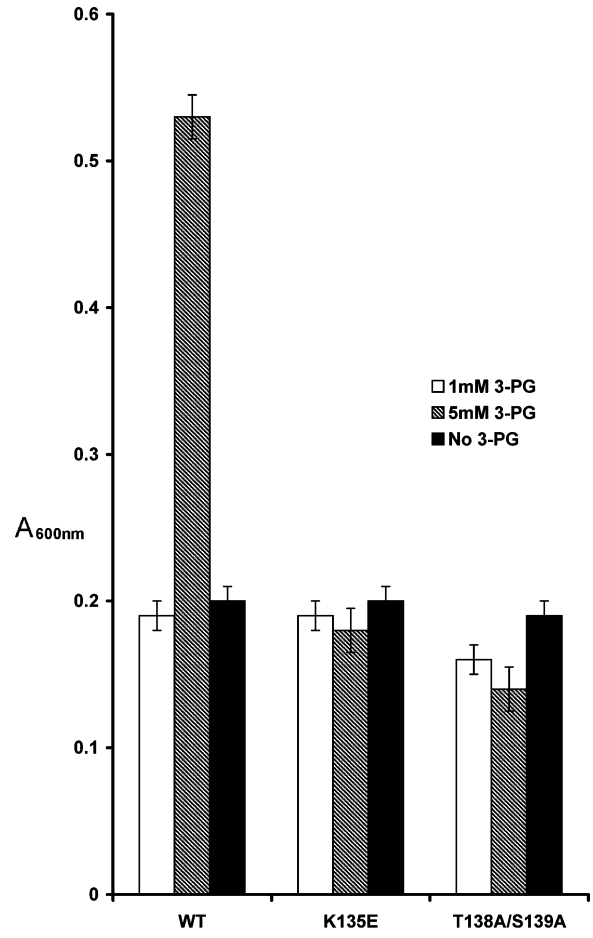

FIGURE 2: Effect of 3-PG on the growth of *C. jejuni*. The wild-type form of PEB3 and the two mutants were grown in minimal medium with 0, 1, or 5 mM 3-PG for 24 h at 37 °C, in triplicate.

Fluorescence Assay for Ligand Binding. Addition of either 3-PG, PEP, or phosphate resulted in a significant increase in the intrinsic fluorescence emission of PEB3 (Figure 1B). Titrations to determine the K_d of these ligands were carried out after dialyses were performed to remove adventitious ligands, e.g., the phosphate that was observed in the PEB3 structure where no ligand had been added (see below). Titration of PEB3 with 2−20 mM citrate did not show any change in protein fluorescence emission (data not shown). To eliminate the possibility of nonspecific fluorescence changes being caused by these ligands, the fluorescence emission of BSA was also measured with the ligands at a final concentration of 2 mM, and no fluorescence emission change was observed. The calculated K_d values for 3-PG, PEP, and phosphate based on these data were 187, 195, and 382 μM, respectively. In the case of aconitate, fluorescence quenching of PEB3 was observed, and a control experiment with BSA showed an even greater quenching effect, indicating that aconitate binding is nonspecific. Two other anions were tested; molybdate also quenched the intrinsic fluorescence, while sulfate had a lower affinity than phosphate, 670 μM. In the absence of crystallographic data, it cannot be assumed that this weak binding was at the same site, however.

Effect of 3-Phosphoglycerate on Bacterial Growth. Addition of 5 mM 3-PG to *C. jejuni* cultured in minimal medium gave an ~2.5-fold enhancement of growth (Figure 2). Control experiments with the two PEB3 isogenic mutants, K135E-His_6 and T138A/S139A, showed no enhancement of growth in the presence of 3-PG, with the final culture densities very similar to that of the wild type in the absence of the ligand.

Crystal Structures of PEB3−Ligand Complexes. All of the PEB3−ligand complexes exhibited good density for the expected ligand. However, in the case of aconitate, the electron density indicated the presence of a phosphate ion rather than that of aconitate. For the "ligand-free" crystals grown from ammonium acetate, we expected no bound ligand; however, clear electron density consistent with a bound phosphate ion was observed, suggesting that this ligand must have copurified with the protein. Structures of PEB3 without added ligand or with aconitate are essentially the same as that of PEB3 crystallized in the presence of phosphate and will not be described further. Structures were obtained for PEB3 cocrystallized with 3-PG, PEP, or phosphate and refined against data to 2.2, 1.7, and 1.6 Å resolution, respectively (Table 1). In the case of PEP, we originally interpreted the electron density to be consistent with this ligand. However, more careful analysis of the electron density for the ligand revealed it to be inconsistent with the expected sp2 geometry about the C2 atom for PEP, appearing instead to have sp3 geometry. We therefore conclude that this complex contains bound L-phospholactate

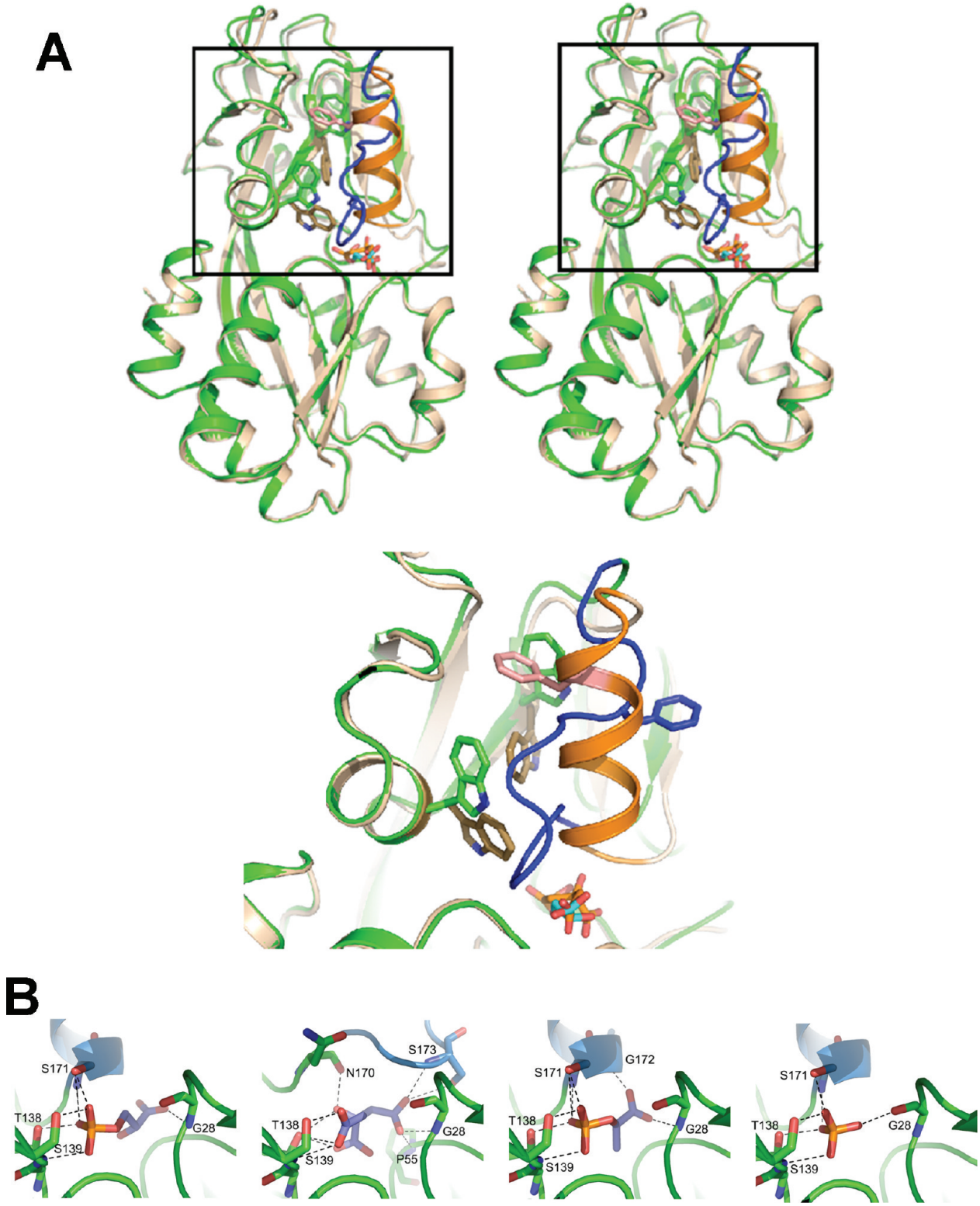

FIGURE 3: Comparison of PEB3 structures. (A) Stereo image of PEB3 bound to 3-PG (wheat) showing the helical structure in the Ser171−Gln180 region in comparison to that of wild-type PEB3 (PDB entry 2HXW) bound to citrate (green/blue). The enlarged region below shows the details of the Ser171−Gln180 region, i.e., the α-helical conformation in the presence of bound 3-PG or extended conformation in the presence of bound citrate, and the different positions of the hydrophobic side chains. (B) Binding site details of the complexes of PEB3 with 3-PG, citrate, L-PL, and phosphate.

(L-PL) rather than PEP, and consistent with this, trace amounts of L-PL were identified by NMR in the commercial PEP preparation we used.

The main difference between these complexes and phosphate species from the previously determined structure of the PEB3−citrate complex is in the conformation of the region of residues 168−183, which now contains an α-helix for residues 171−180 rather than an extended loop (Figure 3A). While no changes in the backbone conformation of other parts of PEB3 occur, significant rotations of the side chains of Trp186 and Trp192 reorganize the hydrophobic area adjacent to the region of residues 168−183 and the side chain

of Arg126 moves significantly to maintain a hydrogen bond with the carbonyl group of Gln182. In this conformation, the bottom of the ligand-binding crevice is narrow, and 3-PG and L-PL fit very tightly. The phosphate is anchored by two hydrogen bonds to Ser171 located in the first turn of the α-helix.

As in other periplasmic transport proteins, the ligand-binding site is formed between the two subdomains of PEB3 and is defined by several loops between secondary structural elements, namely, Pro27−Gly28, Gly54−Pro55, Asn137−Gly140, Pro169−Gly172, and the side chains of Trp189 and Trp192 from an α-helix (Figure 3). The phosphate group of each of these phosphate-containing ligands occupies the same site at the bottom of a deep cleft, formed predominantly by Pro27, Gly28, Thr138, Ser139, Ser171, and Trp192, and forms four direct and four water-mediated hydrogen bonds involving both backbone and side chain atoms. The direct hydrogen bonds involve the side chains of Thr138 and Ser139 and the side chain and carbonyl of Ser171 located in the first turn of an α-helix (Figure 3B). The side chain of Trp192 forms a water-mediated hydrogen bond to the phosphate group. This site appears to be a preferred binding site for a negatively charged group. The remaining part of 3-PG or L-PL fills the rest of the cleft and points toward the solvent. We note that the N-terminus of the 171−180 helix is proximal to the phosphate moiety of the bound ligands, resulting in a favorable dipole effect that would assist in stabilizing their negative charge and potentially play a role in ligand binding (*19*).

In the PEB3−citrate complex, one of the citrate carboxylic groups occupies the same site as the phosphate and engages some of the same residues, Gly28, Thr138, and Ser139, but the bulkiness of the citrate, with an extended hydroxyl group, is not compatible with the narrow binding site (Figure 3C) and would clash with the backbone of Gln172 in a helical conformation of the 171−180 segment. However, citrate fits well into a site created when the 171−180 segment forms a loop. This loop is stabilized by additional hydrogen bonds with citrate involving the backbones of Asn170 and Ser173 as well as the side chain of Ser173. Apart from interactions with the ligand, both conformations of the 168−183 region form many van der Waals and hydrogen bond contacts with neighboring parts of the protein. Thus, this segment of the protein is relatively flexible and can attain at least two conformations in the presence of different ligands.

To investigate whether the 171−180 α-helix is preserved in the absence of bound ligand, we obtained crystals of PEB3 in the absence of added ligand or citrate. Inspection of electron density maps for data from these crystals showed that the ligand-binding site was occupied by a phosphate ion, acquired during cell growth or protein purification. Attempts to obtain the crystal structure of PEB3 in the absence of any bound ligand, i.e., after treatment with higher concentrations of citrate to remove the phosphate, were unsuccessful.

Structure of the K135E Mutant in its Glycosylated Form. The T_{agg} experiments showed only a minor decrease in the thermal stability of the K135E mutant but a loss of its ability to bind 3-PG and PEP. When the K135E mutant *peb3* gene was reintroduced into *Campylobacter*, the expressed protein showed a level of glycosylation at Asn90 of >90%, compared to the level of ∼50% normally observed for PEB3 (*1*). The crystal structure of the K135E glycoprotein was therefore determined, crystallized from the solution containing 0.2 M diammonium hydrogen citrate (*3*). The K135E mutant showed the same overall structure as the previous PEB3−citrate complex (Figure 4A), with a root-mean-square deviation (rmsd) between the refined models of the dimers of 0.22 Å. The conformation of the Val168−Ala183 loop is the same in wild-type PEB3 and in the K135E glycosylated form of the protein. In particular, the conformation of the loop containing the N-glycosylated residue, Asn90, was not affected by attachment of the glycan. The first two sugar residues of the glycan, GalNAcα1,3-diAc-Bac, could be fitted to the electron density linked to Asn90 (Figure 4A).

The mode of citrate binding is the same as previously observed (*3*). The carboxylic group attached to CH2 (CG) of citrate occupies the same site as the phosphate and forms hydrogen bonds with the same residues, Gly28, Thr138, and Ser139. The citrate stabilizes the Val168−Ala183 loop by forming additional hydrogen bonds involving the backbones of Asn170 and Ser173 as well as the side chain of Ser173.

Lys135 is ∼14 Å from the bound ligand and makes no direct contacts with it. Changing Lys135 to Glu alters the dimer interface (Figure 4B), where Lys135 makes a hydrogen bond to Asp84 of the second monomer. There are also bridging water molecules rigidifying the interface, involving the carbonyls of Ala133 and Gly134. In the K135E mutant, the glutamate moves away from the other monomer, and as no bridging water molecules are observed, this interface region is weakened. The mutation also results in a small movement of the backbone of Pro130−Gly134. These residues are in contact with Val168 and Pro169 at the beginning of the flexible 168−183 region. We conclude that these small readjustments in structure affect the conformational preferences of the 168−183 region toward the loop conformation, where phospho ligands would lose two or three hydrogen bonds, in the K135E mutant as compared to the wild type, thereby decreasing their binding affinity. It follows that dimerization plays a subtle but important role in influencing the conformational preferences of the ligand-binding region of PEB3.

Effect of Glycosylation on Stability. In T_m measurements using a SYPRO Orange binding assay, the K135E glycoprotein exhibited a stabilization of 4.7 °C as compared to the nonglycosylated K135E, i.e., 60.3 and 55.6 °C, respectively. The nonglycosylated K135E was slightly less stable than the wild-type PEB3, 57.2 °C (Figure 5).

DISCUSSION

To seek ligands of PEB3, we used both a glycan microarray and DSLS. The glycan microarray has been previously used to identify cell surface ligands for bacterial and fungal adhesins (*6, 20, 21*), but it did not identify a candidate carbohydrate for a PEB3 surface receptor. The only binding was to Man-6-phosphate, although glycoproteins containing this sugar did not bind to PEB3, and it did not stabilize the protein against thermal aggregation. It has not been determined whether the adhesin property of PEB3 is also a function of the central ligand-binding site or of a second region on the molecule. Tests with sulfated Gal and GalNAc species, including the glycan array and DSLS, showed no binding, which suggests that the binding site for phosphates does not function as a recognition site for cell

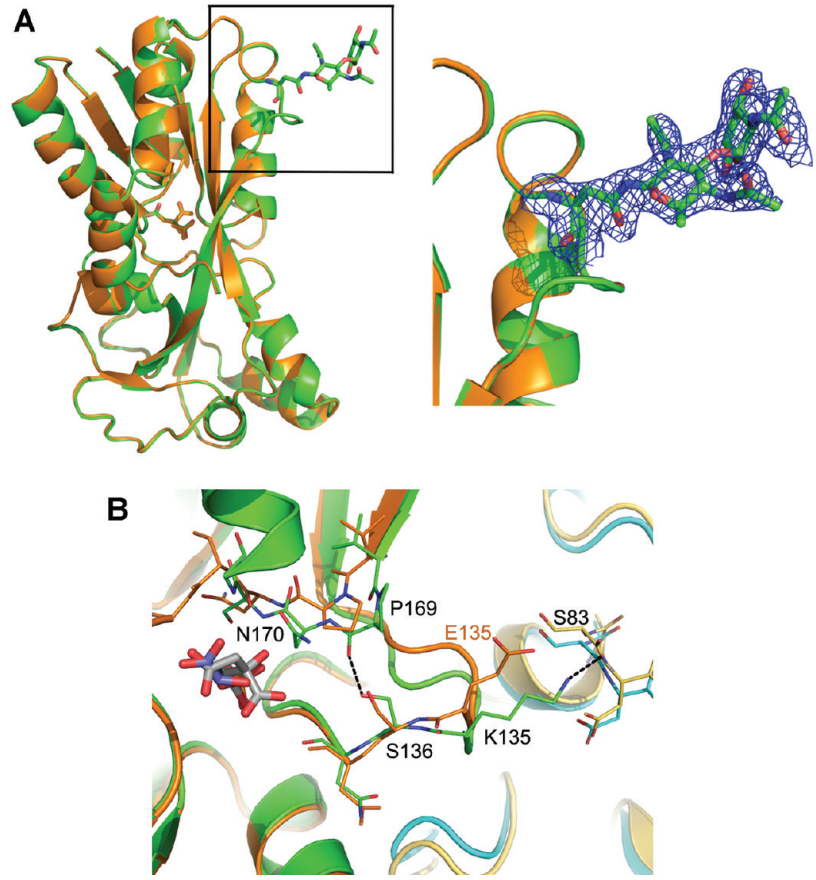

FIGURE 4: Structure of the glycosylated K135E mutant. (A) The wild-type PEB3−citrate complex (gold) and the K135E citrate complex (green) are shown superimposed, with the first two sugar residues of the heptasaccharide glycan, GalNAcα1,3-Bac, covalently attached to Asn90 in K135E. The enlarged portion shows the two sugars fitted into the electron density. (B) Superimposition of the K135E citrate complex and the wild-type 3-PG complex, with the dimer interface H-bonding pattern. H-Bonds formed with the adjacent subunit of the dimer via Ser83′ and Lys135 are not present when this residue is mutated to Glu.

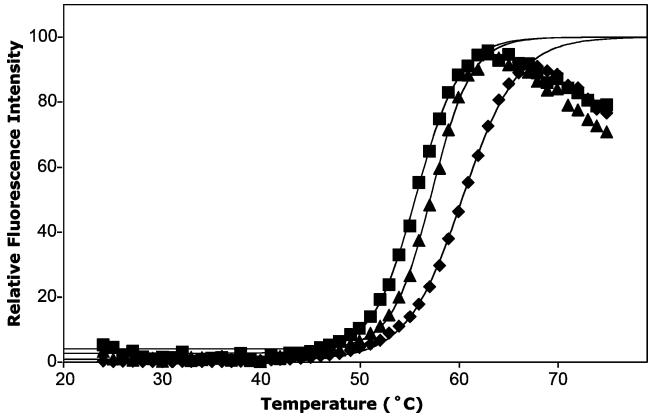

FIGURE 5: Effect of glycosylation on thermal stability. The thermal denaturation behavior of the glycosylated K135E mutant (◆) was compared with that of unglycosylated K135E (■) and wild-type PEB3 (▲), in a fluorescent dye binding assay.

surface-sulfated glycans. Interaction experiments with PEB3 and sulfated glycans such as heparin and other glycosaminoglycans (*18*) are made difficult by the high pI of PEB3, calculated to be 9.3, which leads to strong ionic interactions. PEB1a shares with PEB3 the dual roles of adhesion and transport, in this case transport of Asp and Glu, and its cell surface receptor is also unknown (*5*).

DSLS has proven to be an effective way to identify ligands for proteins of unknown function (*7, 8, 22*). Of the potential ligands that we found by this method, 3-PG appears to be biologically relevant, based on its enhancement of the growth of wild-type *C. jejuni* cells in minimal medium. We therefore propose that PEB3 may function as part of a transport system for 3-PG or other phosphate-containing metabolites, though our combined experiments do not prove this function unequivocally. A transport role for PEB3 was previously suggested on the basis of the similarity of its structure to those of other periplasmic type II transporters (*3*). PEB3 may enhance the growth of *C. jejuni* within host cells by assisting in the uptake of this valuable metabolite from the cytoplasm. This proposal is consistent with the behavior of *C. jejuni* cells lacking PEB3, indicating that PEB3 plays a greater role in colonization than it does in adhesion (*18*). A transporter for 3-PG has been reported in *Salmonella typhimurium* (*23*), but it appears to be of a different structural type than PEB3, as are the several phosphoglycerol transporters that are known (*24*).

The binding constants determined for the three ligands, 3-PG, PEP, and phosphate (~200−400 μM), are weaker than the values usually reported for periplasmic transport proteins, which can be below 1 μM. The Cys transporter Cj0982 has a K_d of 0.14 μM (*25*), and the Asp/Glu transporter PEB1a has K_d values of 0.5 and 0.79 μM for Asp and Glu, respectively (*5*). The K_d values for trivalent ion transporters are higher; e.g., the *E. coli* molybdate transporter that is structurally homologous to PEB3 has a K_d of 3 μM for molybdate and 7 μM for tungstate (*26*). Given the limited number of compounds we screened, it is possible that some

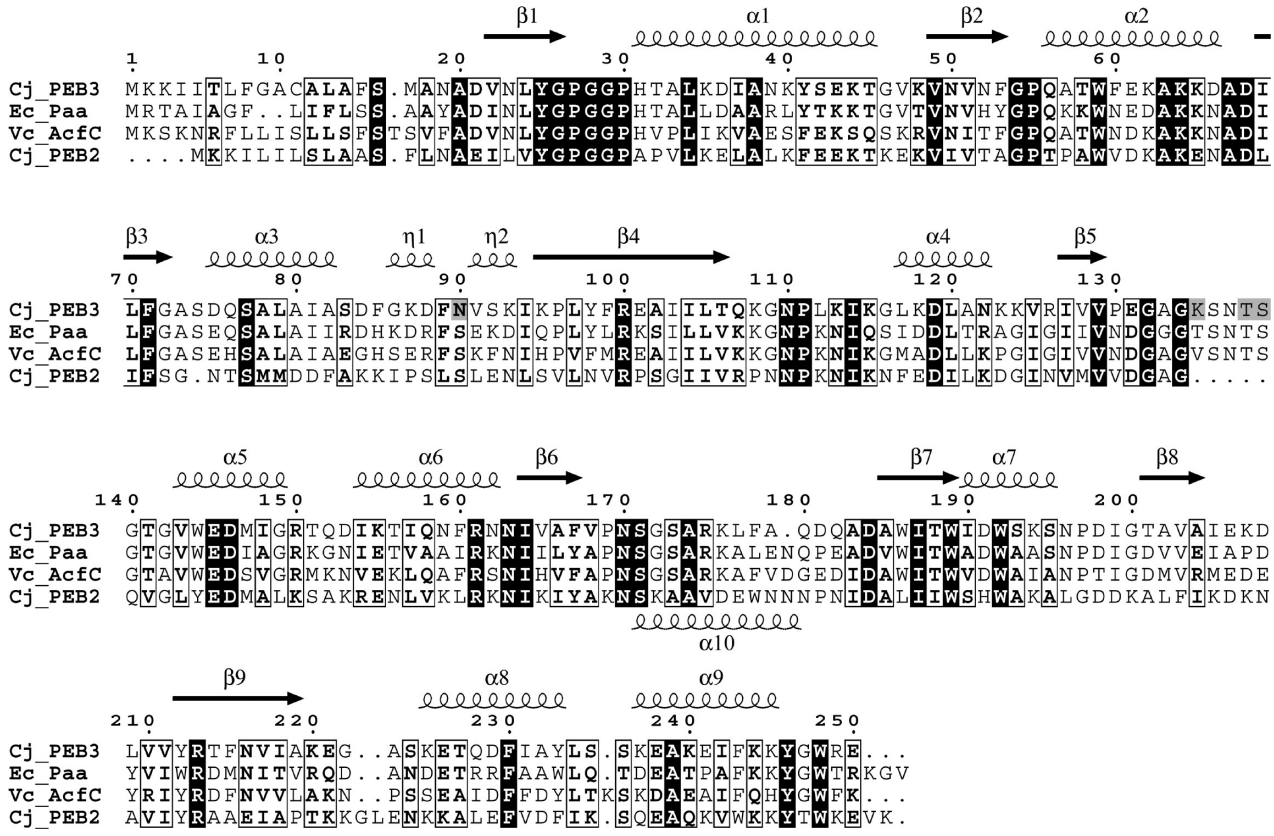

FIGURE 6: Sequence comparisons of PEB3 with PEB2, *E. coli* Paa, and *V. cholera* AcfC (*30*). The alignment was performed with ClustalW2 (*36*) and formatted using ESPript (*37*). The level of sequence identity between PEB3 and Paa is 52% and between PEB3 and AcfC 49%. The structural elements of PEB3 are shown above the alignment, except for the 171−180 helix which is indicated below the alignment and labeled alpha-I0. The glycosylated Asn and the three mutated residues are shaded. The accession numbers for the sequences shown are as follows: Cj_PEB3, gil112359657; Ec_Paa, gil77377457; Vc_AcfC, gil1100875; and Cj_PEB2, gil112360112.

high-affinity ligands were not included in these assays and remained undetected. However, the intracellular concentrations reported for 3-PG are relatively high, e.g., 0.3 μmol/g of wet weight for liver cells, with inorganic phosphate levels more than 15-fold higher (*27*), while concentrations in red cells range from 118 (*28*) to 500 μM (*29*) for 3-PG and are 23 μM for PEP (*28*). Therefore, the binding properties of PEB3 are sufficient to bind these metabolites in the cytoplasm of host cells for transport into colonizing *C. jejuni* bacteria. We did not examine 2-phosphoglycerate, the intermediate compound between 3-PG and PEP in cellular metabolism, but it is also a candidate ligand for PEB3; its cellular level is similar to that of PEP (*29*). L-PL is not a normal cellular component.

Comparison of PEB3 structures bound to various ligands showed that the Val168−Ala183 region assumes two different conformations. In the presence of citrate, this region forms an irregular loop as shown both previously (*3*) and in this study. Here, we have shown that in the presence of phospho ligands, this segment adopts an α-helix encompassing residues 171−180.

This helix increases the overall degree of structural similarity of PEB3 to other type II transport proteins such as the molybdate (PDB entry 1WOD) and sulfate (PDB entry 1SBP) transporters. However, the later are monomeric proteins, while PEB3 is a dimer. Ligand-free structures for these transporters have not been reported, so it cannot be determined if they also undergo similar ligand-dependent conformational changes. It is possible that the flexibility of the 168−183 segment may have a functional role in delivering ligand to the transmembrane component of a transport complex; i.e., a change in its conformation induced by association with the transmembrane protein component could aid release of the ligand for transport.

The ligand binding properties of the T138A/S139A mutant differ from those of the wild type in that, as shown by DSLS, fluorescence, and in vivo bacterial growth experiments, they have lost the ability to bind phospho ligands. This was expected for the T138A/S139A PEB3 mutant and confirmed that these side chains make crucial interactions with the phosphate group. Since the key residues of the PEB3 ligand-binding site, Thr138 and Ser139, are preserved in the sequences of two proteins whose homology to PEB3 was previously reported (*30*), the EPEC *E. coli* adhesin Paa (*30*) and *Vibrio cholerae* colonization factor AcfC (*31*), these proteins may also transport the same ligand(s). In contrast, PEB2, while showing sufficient homology to indicate that it also has the structure of a periplasmic transport protein, differs in the residues predicted to line the ligand-binding site and in the 171−180 helix region (Figure 6). The third member of the PEB group of major *C. jejuni* antigens, PEB1a is a transporter for Asp and Glu (*5*), and its crystal structure showed it is also in the type II family (*32*). However, it is a monomeric protein and more distant in sequence homology, being <20% identical to either PEB3 or PEB2. PEB2 and PEB1a do not have any glycosylation sites, though another transporter protein, Cj0982c, specific for Cys (*25*), is glycosylated on an exposed sequon loop (*2, 3*).

The second mutation, K135E, affects the ligand binding characteristics of PEB3 by disruption of the dimer interface. The high level of glycosylation of this mutant when expressed in *C. jejuni* gave a sufficiently homogeneous preparation for successful crystallization of the glycoprotein. Its structure showed that glycosylation had very little effect on the structure of the protein, including the loop that contains the bound glycan at Asn90. However, glycosylation did stabilize the protein against thermal denaturation by 4.7 °C as compared to unglycosylated K135E PEB3 (Figure 5). While the glycan may therefore be stabilizing the loop around Asn90 in its preferred orientation, it projects away from the protein surface, and there are no H-bonds between the first sugar moiety and the peptide, unlike the structures of some eukaryotic glycoproteins (*33*). The key residues of the sequon, D-F-N^{90}-V-S (*2*), remain exposed on the molecule's surface, and as predicted from this feature of the structure of the nonglycosylated protein (*3*), the folded form of the protein could be glycosylated in vitro by the oligosaccharyltransferase, PglB, with its donor heptasaccharide lipid (M. Feldman and M. Ielmini, personal communication). Only the first two residues of the heptasaccharide, GalNAcα1,3-diAcBac, could be fitted to the electron density; however, this is the first crystal structure obtained for a bacterial N-linked glycoprotein, and only a few bacterial O-linked glycoprotein structures are known, e.g., *Neisseria gonorrheae* pilin (*34*) and *Flavobacter heparinum* chondroitinase B (*35*).

ACKNOWLEDGMENT

We thank Dr. David Smith (Emory University, Atlanta, GA) for the Core H glycan array experiment, Agnès Journet (CEA Grenoble, Grenoble, France) for providing lysosomal proteins for blotting experiments with PEB3, Dr. Omkar Ijare (Institute for Biodiagnostics, National Research Council of Canada, Winnipeg, MB) for helpful information on the cytoplasmic levels of phosphorylated metabolites, Dr. Mario Feldman and Dr. Maria Ielmini (University of Alberta, Edmonton, AB) for examining the glycosylation of PEB3 in vitro, Dr. Harold Jarrell for NMR spectroscopy, Sonia Leclerc for excellent technical assistance, and Dr. Stephane Raymond for his assistance with the Octave software package. This is NRCC publication 49599.

REFERENCES

1. Young, N. M., Brisson, J. R., Kelly, J., Watson, D. C., Tessier, L., Lanthier, P. H., Cadotte, N., St. Michael, F., Aberg, E., and Szymanski, C. M. (2002) Structure of the N-linked glycan present on multiple glycoproteins in the Gram-negative bacterium *Campylobacter jejuni*. *J. Biol. Chem. 277*, 42530–42539.
2. Kowarik, M., Young, N. M., Numao, S., Schulz, B. L., Hug, I., Callewaert, N., Mills, D. C., Watson, D. C., Hernandez, M., Kelly, J. F., Wacker, M., and Aebi, M. (2006) Definition of the bacterial *N*-glycosylation site consensus sequence. *EMBO J. 25*, 1957–1966.
3. Rangarajan, E. S., Bhatia, S., Watson, D. C., Munger, C., Cygler, M., Matte, A., and Young, N. M. (2007) Structural context for protein *N*-glycosylation in bacteria: The structure of PEB3, an adhesin from *Campylobacter jejuni*. *Protein Sci. 16*, 990–995.
4. Parkhill, J., Wren, B. W., Mungall, K., Ketley, J. M., Churcher, C., Basham, D., Chillingworth, T., Davies, R. M., Feltwell, T., Holroyd, S., Jagels, K., Karlyshev, A. V., Moule, S., Pallen, M. J., Penn, C. W., Quail, M. A., Rajandream, M. A., Rutherford, K. M., van Vliet, A. H., Whitehead, S., and Barell, B. G. (2000) The genome sequence of the food-borne pathogen *Campylobacter jejuni* reveals hypervariable sequences. *Nature 413*, 665–668.
5. Leon-Kempis, M. d. R., Guccione, E., Mulholland, F., Williamson, M. P., and Kelly, D. J. (2006) The *Campylobacter jejuni* PEB1a adhesin is an aspartate/glutamate-binding protein of an ABC transporter essential for microaerobic growth on dicarboxylic acids. *Mol. Microbiol. 60*, 1262–1275.
6. http://www.functionalglycomics.org/glycomics/publicdata/selectedScreens.jsp.
7. Kurganov, B. I. (2002) Kinetics of protein aggregation. Quantitative estimation of the chaperone-like activity in test-systems based on suppression of protein aggregation. *Biochemistry (Moscow) 67*, 409–422.
8. Vedadi, M., Niesen, F., Allali-Hassani, A., Federov, O. Y., Finerty, P. J., Wasney, G. A., Yeung, R., Arrowsmith, C., Ball, L. J., Berglund, H., Hui, R., Marsden, B., Nordlund, P., Sundstrom, M., Weigelt, J., and Edwards, A. E. (2006) Chemical screening methods to identify ligands that promote protein stability, protein crystallization, and structure determination. *Proc. Natl. Acad. Sci. U.S.A. 103*, 15835–15840.
9. Pflugrath, J. W. (1999) The finer things in X-ray diffraction data collection. *Acta Crystallogr. D55*, 1718–1725.
10. Collaborative Computational Project, Number 4 (1994) The CCP4 suite: Programs for protein crystallography. *Acta Crystallogr. D50*, 760–763.
11. Otwinowski, Z., and Minor, W. (1997) Processing of X-ray diffraction data collected in oscillation mode. *Methods Enzymol. 276*, 307–326.
12. Navaza, J. (2001) Implementation of molecular replacement in AmoRe. *Acta Crystallogr. D57*, 1367–1372.
13. Murshudov, G. N., Vagin, A. A., Lebedev, A., Wilson, K. S., and Dodson, E. J. (1999) Efficient anisotropic refinement of macromolecular structures using FFT. *Acta Crystallogr. D55*, 247–255.
14. Emsley, P., and Cowtan, K. (2004) Coot: Model-building tools for molecular graphics. *Acta Crystallogr. D60*, 2126–2132.
15. Berman, H. M., Westbrook, J., Feng, Z., Gilliland, G., Bhat, T. N., Weissig, H., Shindyalov, I. N., and Bourne, P. E. (2000) The Protein Data Bank. *Nucleic Acids Res. 28*, 235–242.
16. Matulis, D., Kranz, J. K., Salemme, F. R., and Todd, M. J. (2005) Thermodynamic stability of carbonic anhydrase: Measurements of binding affinity and stoichiometry using ThermoFluor. *Biochemistry 44*, 5258–5266.
17. Neisen, F. H., Berglund, H., and Vedadi, M. (2007) The use of differential scanning fluorimetry to detect ligand interactions that promote protein stability. *Nat. Protoc. 2*, 2212–2221.
18. Langdon, R. H., Linton, D., Hinchcliff, S., Cawthraw, S., Newell, D., and Wren, B. (2007) Characterisation of the *Campylobacter jejuni* major antigenic protein PEB3. *Zoonoses Public Health 54* (Suppl. 1), 100–101 (P297).
19. Sarker, K. D., and Hardman, J. K. (1999) Affinities of phosphorylated substrates for the *E. coli* tryptophan synthase α-subunit: Roles of Ser-235 and helix-8 dipole. *Proteins 21*, 130–139.
20. Chessa, D., Dorsey, C. W., Winter, M., and Bäumler, A. J. (2008) Binding specificity of *Salmonella* plasmid-encoded fimbriae assessed by glycomics. *J. Biol. Chem. 283*, 8118–8124.
21. Zupancic, M. L., Frieman, M., Smith, D., Alvarez, R. A., Cummings, R. D., and Cormack, B. P. (2008) Glycan microarray analysis of *Candida glabrata* adhesin ligand specificity. *Mol. Microbiol. 68*, 547–559.
22. Senisterra, G. A., Markin, E., Yamazaki, K., Hui, R., Vedadi, M., and Awrey, D. E. (2006) Screening for ligands using a generic and high-throughput light-scattering-based assay. *J. Biomol. Screening 11*, 940–948.
23. Varadhachary, A., and Maloney, P. C. (1991) Reconstitution of the phosphoglycerate transport protein of *Salmonella typhimurium*. *J. Biol. Chem. 266*, 130–135.
24. Lemieux, M. J., Huang, Y., and Wang, D.-N. (2004) The structural basis of substrate translocation by the *Escherichia coli* glycerol-3-phosphate transporter: A member of the major facilitator superfamily. *Curr. Opin. Struct. Biol. 14*, 405–412.
25. Muller, A., Thomas, G. H., Horler, R., Brannigan, J. A., Blagova, E., Levdikov, V. M., Fogg, M. J., Wilson, K. S., and Wilkinson, A. J. (2005) An ATP-binding cassette-type cysteine transporter in *Campylobacter jejuni* inferred from the structure of an extracytoplasmic solute receptor protein. *Mol. Microbiol. 57*, 143–155.
26. Hu, Y., Rech, S., Gunsalus, R. P., and Rees, D. C. (1997) Crystal structure of the molybdate binding protein ModA. *Nat. Struct. Biol. 4*, 703–707.
27. Guynn, R. W., Merrill, D. K., and Lund, K. (1986) The reactions of the phosphorylated pathway of L-serine biosynthesis: Thermodynamic relationships in rat liver *in vivo*. *Arch. Biochem. Biophys. 245*, 204–211.

28. Fokina, K. V., Dainyak, M. B., Nagradova, N. K., and Muronetz, V. I. (1997) A study on the complexes between human erythrocyte enzymes participating in the conversions of 1,3-diphosphoglycerate. *Arch. Biochem. Biophys. 345*, 185–192.
29. Minakami, S., and Yoshikawa, H. (1965) Thermodynamic considerations on erythrocyte glycolysis. *Biochem. Biophys. Res. Commun. 18*, 345–349.
30. Batisson, I., Guimond, M.-P., Girard, F., An, H., Zhu, C., Oswald, E., Fairbrother, J. M., Jacques, M., and Harel, J. (2003) Characterization of the novel factor Paa involved in the early steps of the adhesion mechanism of attaching and effacing *Escherichia coli*. *Infect. Immun. 71*, 4516–4525.
31. Hughes, K. J., Everiss, K. D., Kovach, M. E., and Peterson, K. M. (1995) Isolation and characterization of the *Vibrio cholerae acfA* gene, required for efficient intestinal colonization. *Gene 156*, 59–61.
32. Muller, A., Leon-Kempis, M. d. R., Dodson, E., Wilson, K. S., Wilkinson, A. J., and Kelly, D. J. (2007) A bacterial virulence factor with a dual role as an adhesin and a solute-binding protein: The crystal structure at 1.5 Å of the PEB1a protein from the foodborne human pathogen *Campylobacter jejuni*. *J. Mol. Biol. 372*, 160–171.
33. Petrescu, A.-J., Milac, A.-L., Petrescu, S. M., Dwek, R. A., and Wormald, M. R. (2004) Statistical analysis of the protein environment of *N*-glycosylation sites: Implications for occupancy, structure, and folding. *Glycobiology 14*, 103–114.
34. Parge, H. E., Forest, K. T., Hickey, M. J., Christensen, D. A., Getzoff, E. D., and Tainer, J. A. (1995) Structure of the fibre-forming protein pilin at 2.6 Å resolution. *Nature 378*, 32–38.
35. Huang, W., Matte, A., Li, Y., Kim, Y. S., Linhardt, R. J., Su, H., and Cygler, M. (1999) Crystal structure of chondroitinase B from *Flavobacterium heparinum* and its complex with a disaccharide product at 1.7 Å resolution. *J. Mol. Biol. 294*, 1257–1269.
36. Larkin, M. A., Blackshields, G., Brown, N. P., Chenna, R., McGettigan, P. A., McWilliam, H., Wallace, I. M., Wilm, A., Lopez, R., Thompson, J. D., Gibson, T. J., and Higgins, D. G. (2007) Clustal W and Clustal X version 2.0. *Bioinformatics 23*, 2947–2948.
37. Gouet, P., Courcelle, E., Stuart, D. I., and Metoz, F. (1999) ESPript: Analysis of multiple sequence alignments in PostScript. *Bioinformatics 15*, 305–308.

BI802195D